An $\alpha_{IIb}\beta_3$- and phosphatidylserine (PS)-binding recombinant fusion protein promotes PS-dependent anticoagulation and integrin-dependent antithrombosis

Received for publication, October 10, 2018, and in revised form, February 10, 2019 Published, Papers in Press, February 25, 2019, DOI 10.1074/jbc.RA118.006044

Jian Jing[1] **and Yanna Sun**

From the Beijing Key Laboratory of Genetic Engineering and Biotechnology, College of Life Sciences, Beijing Normal University, Xinwai St. 19, Haidian District, Beijing 100875, China

Edited by George M. Carman

Blood platelets are required for normal wound healing, but they are also involved in thrombotic diseases, which are usually managed with anticoagulant drugs. Here, using genetic engineering, we coupled the disintegrin protein echistatin, which specifically binds to the platelet integrin $\alpha_{IIb}\beta_3$ receptor, to annexin V, which binds platelet membrane-associated phosphatidylserine (PS), to create the bifunctional antithrombotic molecule recombinant echistatin–annexin V fusion protein (*r*-EchAV). Lipid binding and plasma coagulation studies revealed that *r*-EchAV dose-dependently binds PS and delays plasma clotting time. Moreover, *r*-EchAV inhibited ADP-induced platelet aggregation in a dose-dependent manner and exhibited potent antiplatelet aggregation effects. *r*-EchAV significantly prolonged activated partial thromboplastin time, suggesting that it primarily affects the *in vivo* coagulation pathway. Flow cytometry results indicated that *r*-EchAV could effectively bind to the platelet $\alpha_{IIb}\beta_3$ receptor, indicating that *r*-EchAV retains echistatin's receptor-recognition region. *In vivo* experiments in mice disclosed that *r*-EchAV significantly prolongs bleeding time, indicating a significant anticoagulant effect *in vivo* resulting from the joint binding of *r*-EchAV to both PS and the $\alpha_{IIb}\beta_3$ receptor. We also report optimization of the *r*-EchAV production steps and its purification for high purity and yield. Our findings indicate that *r*-EchAV retains the active structural regions of echistatin and annexin V and that the whole molecule exhibits multitarget-binding ability arising from the dual functions of echistatin and annexin V. Therefore, *r*-EchAV represents a new class of anticoagulant that specifically targets the anionic membrane-associated coagulation enzyme complexes at thrombogenesis sites and may be a potentially useful antithrombotic agent.

Platelets are irregular fragments formed by megakaryocytes and play an important role in hemostasis, thrombosis, and inflammation. When endothelial cells are damaged, platelets are activated and adhere to the collagen fibers exposed to the injured site. The factors affecting platelet adhesion include platelet membrane glycoprotein, collagen of endothelial tissue (collagen), and hemophilia factor (von Willebrand factor). Adherent platelets release ADP, thromboxane A2, 5-hydroxytryptamine, and other contents to promote platelet activation (1, 2). At this point, multiple signaling pathways are initiated and interact with each other, and the internal signal mechanism is amplified to activate the platelet surface $\alpha_{IIb}\beta_3$ receptor. The damaged endothelial tissue releases coagulation factor III to activate the exogenous coagulation pathway, and the local platelets produce thrombin quickly, causing more platelet aggregation, forming a softer hemostatic embolus (3).

Platelets play an important role in normal wound healing and are also important causes of pathological thrombotic diseases. Thrombotic diseases are characterized by high morbidity, disability, and mortality and seriously endanger human life and health. Anticoagulant and antithrombotic drugs play an important role in the prevention and treatment of thrombotic diseases. To achieve high-efficiency antithrombosis, until recently most clinical guidelines recommended both anticoagulation and dual antiplatelet therapy (triple therapy) (4, 5). Personalized detection, treatment, and evaluation are also the current research hot spots of antithrombotic therapeutic agents.

To improve the efficacy of the drug while not increasing the amount of drug used and reducing drug use costs, we attempted to couple echistatin (ECH),[2] which specifically binds to the platelet $\alpha_{IIb}\beta_3$ integrin receptor, with annexin V (ANV), which specifically binds to the platelet membrane PS molecule, by genetic engineering techniques to form an efficient bifunctional recombinant antithrombotic molecule *r*-EchAV.

PS accounts for ~2–10% of the total lipid content of cells (6) and is often considered a "fingerprint" molecule for apoptotic cells (7, 8). It must be mentioned here that PS is also a fingerprint molecule of activated platelets (9, 10). When the platelets

This work was supported by Joint Construction Project of the Beijing Education Committee to Beijing Normal University No. 2017110651103 and Grant BNU10300104977 (to J. J.) from the Young Scholars Fund of Beijing Normal University. The authors declare that they have no conflicts of interest with the contents of this article.

The nucleotide sequence(s) reported in this paper has been submitted to the GenBank™/EBI Data Bank with accession number(s) MK681867.

[1] To whom correspondence should be addressed. Tel.: 86-010-58802065; E-mail: jjing@bnu.edu.cn.

[2] The abbreviations used are: ECH, echistatin; ANV, annexin V or annexin A5; aPTT, activated partial thromboplastin time; DAV, diannexin; FIB, fibrinogen assay; IPTG, isopropyl β-D-thiogalactopyranoside; PC, phosphatidylcholine; PPP, platelet-poor plasma; PRP, platelet-rich plasma; PS, phosphatidylserine; PSP, prescission protease; PT, plasma clotting time; SPR, surface plasmon resonance; TT, thrombin time; GST, GSH *S*-transferase; TEMED, *N*,*N*,*N*′,*N*′-tetramethylethylenediamine; *r*-EchAV, recombinant echistatin–annexin V fusion protein; SEC, size-exclusion chromatography; TDD, targeted drug delivery; FVa, factor Va; FXa, factor Xa; KPI, Kunitz-type protease inhibitor; sTF, soluble tissue factor; HRP, horseradish peroxidase.

change from a resting state to an activated state, the PS molecules originally located in the inner membrane of the cells are largely translocated to the outside of the cell membrane. The flipping of the PS will initiate or directly participate in physiological processes such as coagulation or phagocytosis. The PS-rich platelet surface catalyzes the onset of coagulation and ultimately leads to the formation of thrombin, which in turn stabilizes platelet-rich thrombotic tissue through fibrin formation (3).

ANV, a nonglycosylated single-chain protein discovered as a class of anticoagulant proteins of vascular tissue (11), is a member of the annexin family of calcium-dependent phospholipid-binding proteins and binds with very high affinity to PS-containing phospholipid bilayers (12–15). ANV also binds to human platelets with a K_d of 7 nM (16, 17). Binding to quiescent platelets *in vitro* is minimal, although maximally stimulated platelets contain nearly 200,000 ANV-binding sites; this substantially exceeds the number of binding sites for antibodies to integrin $\alpha_{IIb}\beta_3$ (~25,000 on activated platelets) (18). Anticoagulant effects can be achieved by competitively binding PS sites (19, 20). ANV exerts antithrombotic activity by binding to PS, inhibiting the activation of serine proteases important in blood coagulation. ANV is a relatively small protein (M_r 36,000) that is easily produced in quantity by recombinant DNA methods. It has been shown that recombinant ANV has the same PS-binding ability as the native state of ANV present in human tissues (21–23), and as a human protein it would not be expected to induce an immune response, unlike murine monoclonal antibodies. It is also virtually absent from normal human plasma (24) because it rapidly passes from the blood into the kidneys due to its relatively small size.

How to couple different mechanisms to achieve a multieffect therapy is an important direction of antithrombotics or anticoagulant research and development. Therefore, rational coupling of different mechanisms of action to design fusion proteins has become the key to successful research. We constructed the ECH-linker–ANV recombinant fusion protein (*r*-EchAV) by genetic engineering technology. ECH can efficiently bind to the integrin receptor $\alpha_{IIb}\beta_3$ exposed on the surface of activated platelets, inhibiting platelet aggregation efficiently to achieve an antithrombotic effect; ANV binds a large number of PS molecules valgus to the surface of activated platelets in a calcium-dependent manner. We hope that the constructed *r*-EchAV can simultaneously couple the above two anticoagulant/antithrombotic mechanisms to become a bifunctional antithrombotic recombinant protein molecule. This paper describes the phospholipid binding and platelet integrin receptor binding characteristics of *r*-EchAV, and its anticoagulant effect *in vivo* was evaluated based on animal models. The preparation process and physicochemical characteristics of *r*-EchAV were also studied and elaborated.

Results

Construction and expression of recombinant r-EchAV fusion protein

The DNA fragments containing the constructed ECH gene and the *rh*-ANV gene were further amplified and subjected to agarose gel electrophoresis, and the detection results are shown in Fig. 1*A*. These results showed that the DNA size met the expected requirements. Combined with the results of DNA sequencing, it can be confirmed that the base sequence of the DNA fragment of the ECH gene or the ANV gene is completely correct. The translated amino acid sequences of these synthetic genes match the published sequence of ANV and ECH listed in the GenBank™ database.

The ECH-L and L-ANV genes were used as templates, and E3F and LAA-3 were used as primers for upstream and downstream, respectively; PCR was carried out to construct a 1226-bp DNA fragment containing the *r*-EchAV gene (as shown in the Fig. 1*B*). After DNA sequencing, the base sequence was confirmed to be completely correct and to conform to the expected base sequence requirement of the recombinant *r*-EchAV gene; its nucleotide sequence thereof is shown in Table 1*B*. The *r*-EchAV gene was finally cloned into the pGEX vector, and soluble expression was achieved in *Escherichia coli*. Furthermore, we explored and optimized the bacterial culture and important induction expression conditions of the recombinant *r*-EchAV fusion protein and placed a good foundation for successful follow-up preparation of the *r*-EchAV.

The optimal IPTG dosage in the induction of *r*-EchAV expression is shown in Fig. 2*A*. Our studies showed that under the conditions of different IPTG concentrations in the medium, significant amounts of expression products were induced, with a size of 70 kDa. The molecular weight of this induced expression product was in accordance with the expected theoretical value of GST–*r*-EchAV (70.1 kDa). However, we also found that when the final concentration of IPTG in the medium reached 100 μM, the expression level of the macromolecule fusion recombinant protein GST–*r*-EchAV also reached its highest value and no longer increased in response to increases in the IPTG concentration. At the same time, considering that an excessive IPTG concentration will promote the formation of inclusion bodies in *E. coli* and that a too high IPTG concentration can also exhibit strong toxicity against *E. coli* cells, we finally determined the optimal concentration of the cell inducer IPTG of *r*-EchAV expression to be 100 μM for subsequent large-scale bacterial culture, induction of expression, and preparation of recombinant proteins.

The experimental identification results of optimal temperature control during *r*-EchAV–induced expression are shown in Fig. 2*B*. The IPTG-induced expression of recombinant *E. coli* was carried out under the control conditions of 37, 30, and 25 °C, respectively. Our studies have shown that under the above temperature conditions, *r*-EchAV expression products could be achieved efficiently and in large quantities; the target recombinant protein expression products were found in both the isolated supernatant and the bacterial inclusion bodies, and the yield of the expressed products was not significantly different. Considering that the formation of *E. coli* inclusion bodies is positively correlated with the temperature, reducing the temperature during induction will help to reduce the formation of bacterial inclusion bodies, so we finally controlled the temperature during the induction of *r*-EchAV at 25 °C and used it as the optimum temperature for the later large-scale *E. coli* culture and *r*-EchAV preparation.

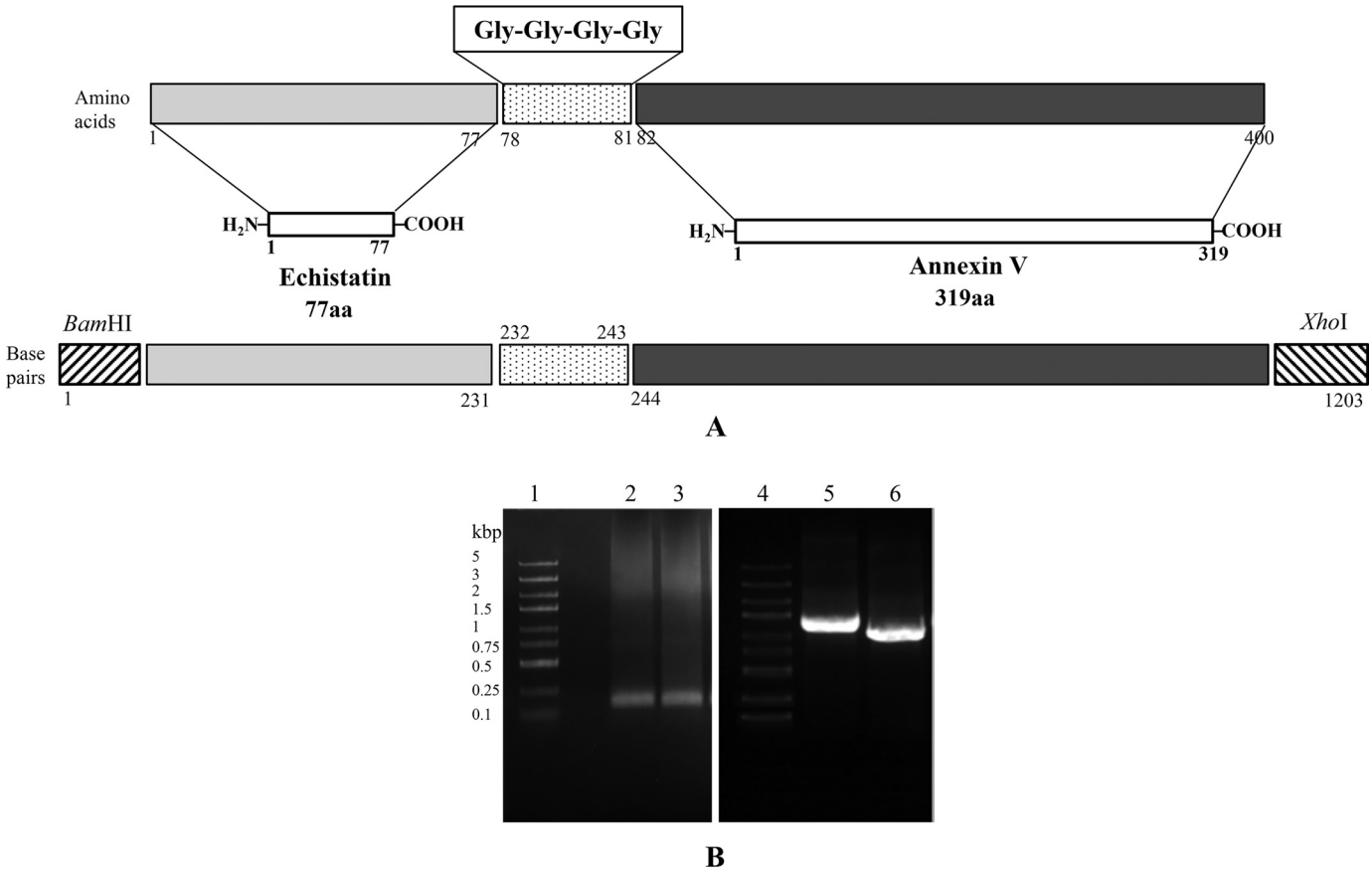

Figure 1. Schematic presentation of echistatin, annexin V, and their fusion product *r*-EchAV (*A*) and PCR screening of the synthesized Ech gene (231 bp), *r*-EchAV gene (1203 bp), and recombinant plasmids pGST–*r*-ANV and pGST–*r*-EchAV (*B*). *Lanes 1* and *4*, DNA molecular mass markers; *lanes 2* and *3*, PCR products of Ech gene; *lanes 5* and *6*, PCR products of recombinant plasmids pGST–*r*-EchAV and pGST–*r*-ANV, respectively.

We also explored the optimal harvest time during the induction of *r*-EchAV expression, as shown in Fig. 2*C*. The results showed that the content of recombinant foreign gene expression products in the whole-cell protein of the bacteria increased gradually with the prolongation of induced expression control times at 0, 5–12, and 20 h. However, we found that when the harvest time was controlled between 11 and 12 h, the recombinant protein content reached its highest value. Further prolongation of the induced expression time decreased the content of the target protein. We speculate that because of the excessive prolongation of the induction time, a degradation tendency of the recombinant expression product is also obvious, resulting in a decrease in target protein content; another reason may be that too long of an induction time will result in decreased utilization of nutrients by *E. coli* cells, excessive accumulation of harmful products, and reduced ability to synthesize foreign proteins in the later stage. Based on the above results, we finally determined that the induction time of *r*-EchAV was controlled within 12 h.

Based on the above studies, recombinant fusion proteins (GST–*r*-EchAV) formed by *r*-EchAV and GST were present in a soluble form in a large amount in the supernatant after disruption of the cells. Therefore, after the induction of expression was completed, the cells were collected by centrifugation and disrupted, and then the supernatant was collected for further purification and property studies.

Purification of r-EchAV from E. coli

Most of the *E. coli*–expressed fusion proteins were found in the inclusion bodies. Fortunately, our expression product was present in a soluble form in *E. coli*. Therefore, the subsequent purification steps circumvent complex and cumbersome steps such as inclusion body extraction and protein de-renaturation. The results are shown in Fig. 2*D*.

Our studies have shown that combined with GST column-affinity chromatography technology, GST–*r*-EchAV recombinant foreign protein was obtained with relatively good purification, and the preparation yield was also relatively high. The purity of the target protein GST–*r*-EchAV was above 92%, and the yield reached 19 mg/liter (as shown in Table 2).

In the specific digestion process of the GST–*r*-EchAV recombinant protein, we explored different substrate/enzyme molecular molar ratios to achieve optimal protease digestion. As shown in Fig. 2*E*, the enzymatic cleavage effect of the PSP enzyme on GST–*r*-EchAV was not enhanced with the increase in the amount of protease. Conversely, we observed that when the molar ratio of the recombinant protein GST–*r*-EchAV to PSP enzyme was 800:1 and the enzyme digestion was 12 h, the enzymatic cleavage effect was very good. GST–*r*-EchAV (70 kDa) can be sufficiently cleaved to form the products *r*-EchAV (44 kDa) and GST (26 kDa). Therefore, in the later large-scale preparation process,

Table 1
Design, synthesis and identification of *r*-EchAV recombinant gene

A. PCR primers.

Ech forward primer 1	5′-GCCGGGTGCTGAATGTGAATCCGGTCCGTGTTGTCGTAACTGTAAATTCC-3′
Ech reverse primer 1	5'-CCACGAGCACGTTTACAGATGGTACCTTCTTTCAGGAATTTACAGTTACG-3'
Ech forward primer 2	5'-GGCTAACCCGTGTTGTGACGCTGCTACCTGTAAACTGCTGCCGGGTGCTG-3'
Ech reverse primer 2	5'-TCACAGGTTTTACCGTTACAGTAGTCGTCCATGTCGTCACCACGAGCACG-3'
Ech-*Bam*HI	5'-CGATGGATCCATGGAAGCTGGTGAAGACTGTGACTGTGGTTCCCCGGCTAACCCG-3'
Ech-(Gly)4	5'-ACCACCACCACCGGTAGCCGGACCTTTGTGCGGGTTACGCGGACAGTCACAGGTTTTACC-3'
ANV forward primer	5′-GATCGGATCCAGTCTGGTCCTGCTTCACCTT-3′
ANV reverse primer	5′-ATCAAGCTTATGCATGTCATCTTCTCCACAGAG-3′
ANV-(Gly)4	5'-GGTGGTGGTGGTGCACAGGTTCTCAGAGGC-3'
ANV-*Xho*I	5'-GCATCTCGAGCTATTAGTCGTCCTCTCC-3'

Restriction enzyme cleavage sites and linker sequence are underlined.

B. The complete nucleotide sequence of the coding frame of the *r*-EchAV recombinant gene final construct.

```
No.
1       ATGGAAGCTG GTGAAGACTG TGACTGTGGT TCCCCGGCTA ACCCGTGTTG TGACGCTGCT  60
61      ACCTGTAAAC TGCTGCCGGG TGCTGAATGT GAATCCGGTC CGTGTTGTCG TAACTGTAAA  120
121     TTCCTGAAAG AAGGTACCAT CTGTAAACGT GCTCGTGGTG ACGACATGGA CGACTACTGT  180
181     AACGGTAAAA CCTGTGACTG TCCGCGTAAC CCGCACAAAG GTCCGGCTAC CGGTGGTGGT  240
241     GGTGCACAGG TTCTCAGAGG CACTGTGACT GACTTCCCTG GATTTGATGA GCGGGCTGAT  300
301     GCAGAAACTC TTCGGAAGGC TATGAAAGGC TTGGGCACAG ATGAGGAGAG CATCCTGACT  360
361     CTGTTGACAT CCCGAAGTAA TGCTCAGCGC CAGGAAATCT CTGCAGCTTT TAAGACTCTG  420
421     TTTGGCAGGG ATCTTCTGGA TGACCTGAAA TCAGAACTAA CTGGAAAATT TGAAAAATTA  480
481     ATTGTGGCTC TGATGAAACC CTCTCGGCTT TATGATGCTT ATGAACTGAA ACATGCCTTG  540
541     AAGGGAGCTG GAACAAATGA AAAAGTACTG ACAGAAATTA TTGCTTCAAG GACACCTGAA  600
601     GAACTGAGAG CCATCAAACA AGTTTATGAA GAAGAATATG GCTCAAGCCT GGAAGATGAC  660
661     GTGGTGGGGG ACACTTCAGG GTACTACCAG CGGATGTTGG TGGTTCTCCT TCAGGCTAAC  720
721     AGAGACCCTG ATGCTGGAAT TGATGAAGCT CAAGTTGAAC AAGATGCTCA GGCTTTATTT  780
781     CAGGCTGGAG AACTTAAATG GGGGACAGAT GAAGAAAAGT TTATCACCAT CTTTGGAACA  840
841     CGAAGTGTGT CTCATTTGAG AAAGGTGTTT GACAAGTACA TGACTATATC AGGATTTCAA  900
901     ATTGAGGAAA CCATTGACCG CGAGACTTCT GGCAATTTAG AGCAACTACT CCTTGCTGTT  960
961     GTGAAATCTA TTCGAAGTAT ACCTGCCTAC CTTGCAGAGA CCCTCTATTA TGCTATGAAG  1020
1021    GGAGCTGGGA CAGATGATCA TACCCTCATC AGAGTCATGG TTTCCAGGAG TGAGATTGAT  1080
1081    CTGTTTAACA TCAGGAAGGA GTTTAGGAAG AATTTTGCCA CCTCTCTTTA TTCCATGATT  1140
1141    AAGGGAGATA CATCTGGGGA CTATAAAAAA GCCCTGCTGC TGCTGTGTGG AGAGGACGAC  1200
1201    TAA
```

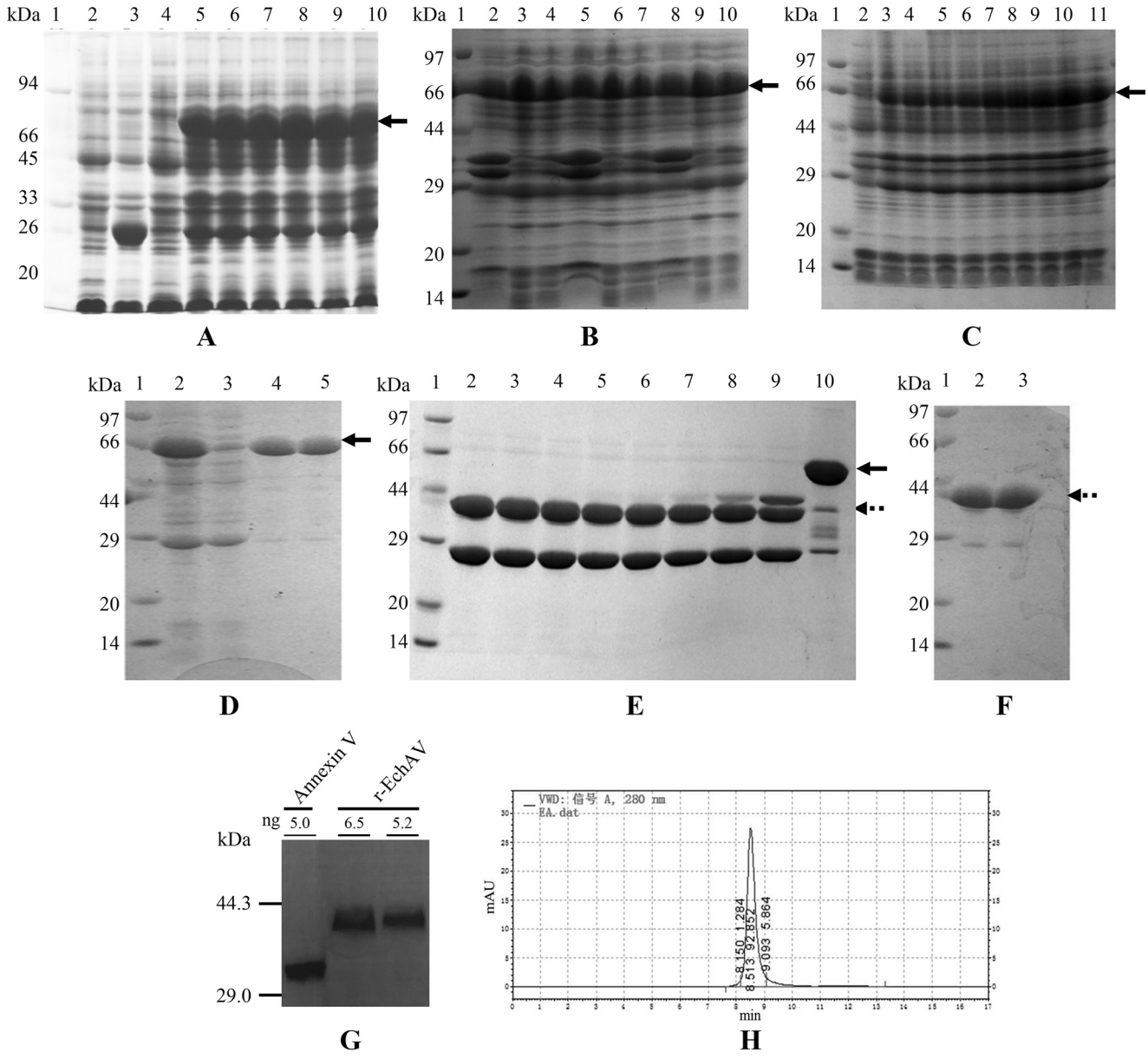

Figure 2. Optimal conditions for inducing the expression, purification, and determination of *r*-EchAV. Samples were analyzed by 12% SLS-PAGE followed by Coomassie Blue staining. All samples were boiled for 3 min with 50 mM DTT. Approximately 10–15 μg of protein was loaded on each lane. The reference range of protein molecular mass is 97–14 kDa. The induced expression band of the target protein is indicated by the *arrow* in *A–C*. *D–F*, GST–*r*-EchAV is shown by the *solid arrow*; *r*-EchAV is shown by the *dotted arrow*. *A,* identification of different concentrations of IPTG as inducer. *Lane 1*, molecular mass markers; *lane 2*, *E. coli*/pGEX-6P-1, no IPTG addition; *lane 3*, *E. coli*/pGEX-6P-1, 100 μM IPTG; *lanes 4–10*, *E. coli*/pGEX-6P–*r*-EchAV, IPTG addition was at different concentrations: 0, 25, 50, 100, 150, 200, and 300 μM, respectively. *B,* identification under different induction temperatures. *Lane 1*, molecular mass markers; *lanes 2–4*, total bacterial protein, supernatant, and inclusion body obtained by induced expression at 37 °C; *lanes 5–7*, total bacterial protein, supernatant, and inclusion body obtained by induced expression at 30 °C; *lanes 8–10*, total bacterial protein, supernatant, and inclusion body obtained by induced expression at 25 °C. *C,* identification after different induction times. *Lane 1*, molecular mass markers; *lanes 2–11*, the total bacterial protein after 0 and 5–12, or 20 h of IPTG induced expression. *D*, purification of induced fusion protein GST–*r*-EchAV by affinity chromatography. *Lane 1*, molecular mass markers; *lane 2*, supernatant after induced expression at 25 °C; *lane 3*, penetrating solution in chromatography; *lanes 4* and *5*, eluted GST–*r*-EchAV. *E,* cleavage efficiency of GST–*r*-EchAV by PSP-specific protease digestion. *Lane 1,* molecular mass markers; *lanes 2–9*, PSP digestion effect (molar ratio of GST–*r*-EchAV to PSP enzyme is 800, 400, 300, 200, 100, 50, 10, and 3, respectively); *lane 10*, fusion protein as a control. *F,* purified *r*-EchAV was identified by 12% SLS-PAGE. *Lane 1,* molecular mass markers; *lanes 2* and *3*, *r*-EchAV. *G,* Western blotting assay of *r*-EchAV (44.1 kDa) and annexin V (35.7 kDa). *H,* SEC-HPLC analysis of *r*-EchAV.

the proportion of substrate/enzyme was controlled at around 800:1 (molar ratio).

Protein determination

Using the anti-human ANV polyclonal antibody, we performed a Western blotting assay on the purified *r*-EchAV recombinant protein. The results are shown in Fig. 2*G*. Our studies have shown that *r*-EchAV exhibits a full ANV antibody-binding effect. This indicates that the *r*-EchAV recombinant fusion protein retains the intact ANV epitope structure.

The experimental results of molecular sieve SEC-HPLC of *r*-EchAV are shown in Fig. 2*H*. Our studies have shown that the absorption peak of the *r*-EchAV protein was detected in the range of 8.150–9.093-min retention time and reached its peak

Table 2

Approximate yield and purity of the total and target proteins after extraction and purification with affinity chromatography and *r*-EchAV after specific digestion and ultrafiltration

The preparation experiments were repeated at least three times.

	GST–*r*-EchAV		GST		*r*-EchAV[b]	
Total protein[a]	Yield	Purity	Yield	Purity	Yield	Purity
mg	*mg*	%	*mg*	%	*mg*	%
275.2 ± 13	36.1 ± 1.6	96	14.7 ± 0.8	99	19.8 ± 1.1	99

[a] The extraction and purification start from 1 liter of bacteria cultured and induced following the method described in the text.
[b] *r*-EchAV was prepared from GST–*r*-EchAV by protease digestion with scissor-protease.

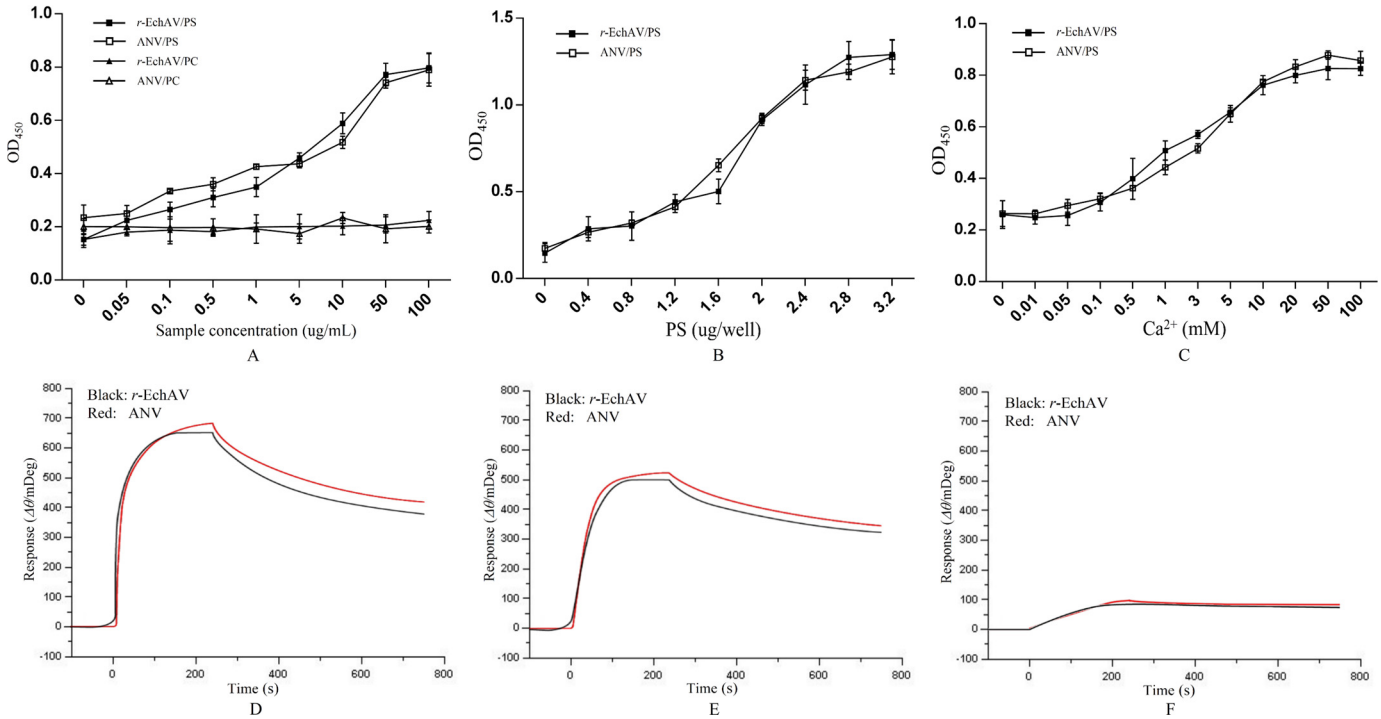

Figure 3. Binding analysis of *r*-EchAV to phospholipids. *A*, binding analysis of *r*-EchAV to different cell membrane phospholipids. *B*, binding analysis of *r*-EchAV to different doses of PS. *C*, effect of Ca^{2+} on the binding of *r*-EchAV to PS. *D–F*, SPR sensorgrams showing the interaction between phospholipids and *r*-EchAV (*black curves*) or ANV (*red curves*) at a concentration of 640, 160, 40 nM, respectively.

at 8.513 min. The peak shape symmetry was good. This result is consistent with the peak time parameter of the molecular mass of the 44-kDa protein identified by SEC-HPLC. The absorption peak-to-peak area percentage of the target protein *r*-EchAV reached 92.852%. This fully demonstrates that the *r*-EchAV recombinant protein exists in a single form; the monomer form is stably present, and no polymer is formed in a solution state. This structural feature is different from that of ANV. ANV can form dimers or even polymers. This suggests that the addition of the ECH structure to the N-terminal of the ANV molecule hinders the intermolecular polymerization of ANV and changes the original polymerization conditions of the ANV molecule. The *r*-EchAV molecule is preferably present in solution in a stable form as a single molecule.

Study on the binding characteristics of r-EchAV fusion protein to phospholipids

r-EchAV/phospholipid binding specificity assay—The test results are shown in Fig. 3*A*. Our studies have shown that *r*-EchAV, like ANV molecules, exhibits different binding abilities to different phospholipids, *i.e.* it does not bind to PC, and the binding effect with PS increases with increasing sample protein concentration, showing a significant dose-dependent relationship. This indicates that the phospholipid-binding properties of *r*-EchAV are not significantly different from those of ANV. This also suggests that the ECH structure in the *r*-EchAV molecule does not block the interaction site of ANV with PS.

r-EchAV/phospholipid binding dose correlation test—The results are shown in Fig. 3*B*. As seen from this figure, when different doses of PS were immobilized in the wells of the ELISA plate, the binding of *r*-EchAV to PS showed a dose-dependent relationship, and at PS >2.5 μg, the protein and PS were gradually saturated.

Effect of calcium ion concentration on r-EchAV/phospholipid binding—The results are shown in Fig. 3*C*. Our studies have shown that the binding activity of *r*-EchAV to PS increases with an increase in Ca^{2+} concentration when the Ca^{2+} concentration is between 0.5 and 10 mM. This finding indicates that the specific binding between the *r*-EchAV molecule and PS requires the presence of Ca^{2+}. This characteristic is similar in nature to ANV. As a calcium ion-dependent phospholipid-binding protein, ANV can reversibly bind to negatively charged PS when Ca^{2+} is present.

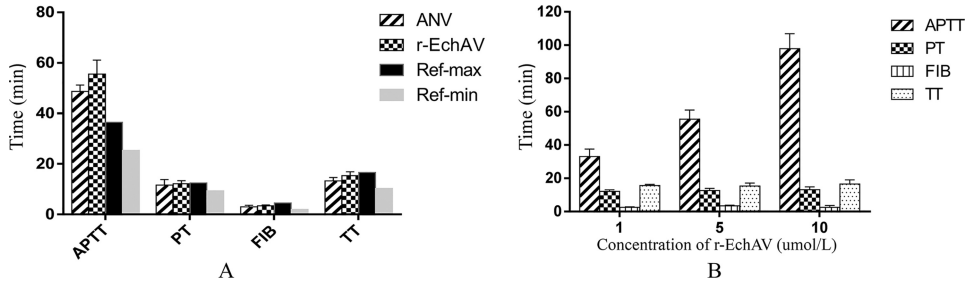

Figure 4. Tetrachoric assay of blood coagulation by *r*-EchAV. *A,* four assessing items of coagulation when the concentration of sample protein (*r*-EchAV or ANV) was 5 μM. *B,* changes in the four assessing items of coagulation under different *r*-EchAV concentrations. The clinical minimum reference value (*Ref-min*) and maximum reference value (*Ref-max*) of APTT, PT, FIB, and TT were 25.4/36.5 (seconds), 9.4/12.5 (seconds), 2.0/4.6 (g/liter), and 10.3/16.6 (seconds), respectively.

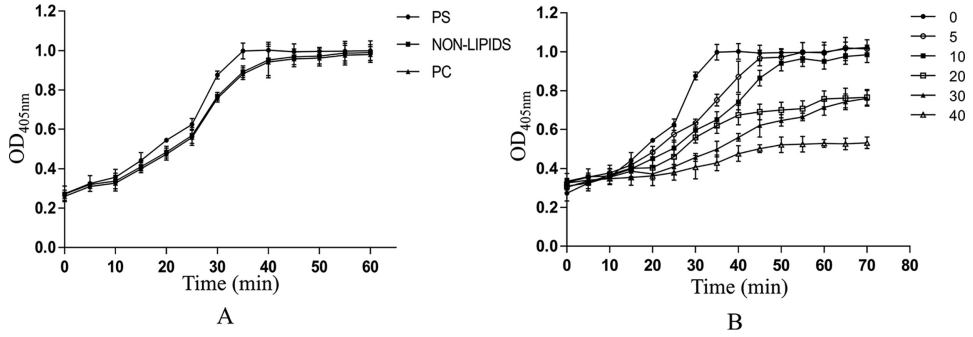

Figure 5. Effect of *r*-EchAV on the plasma coagulation time. Plasma coagulation was initiated by adding $CaC1_2$, and the absorbance at 405 nm was monitored. Each point is the mean ± S.D. of three determinations. *A,* effect of PS or PC alone on plasma coagulation. PS (*closed circles*), PC (*closed triangles*), and nonlipids (*closed squares*), respectively. *B,* effect of *r*-EchAV on the plasma coagulation time with PS was examined. *r*-EchAV (0 μM (*closed circles*), 5 μM (*open circles*), 10 μM (*closed squares*), 20 μM (*open squares*), 30 μM (*closed triangles*), and 40 μM (*open triangles*), respectively) was incubated in lipid-coated microtiter wells in the presence of $CaCl_2$.

Kinetics of interaction between r-EchAV and PS—To determine the binding parameters of the interaction between *r*-EchAV and PS or PC, we performed surface plasmon resonance assays. The preparations of *r*-EchAV or ANV were allowed to flow over the chip in the presence of 2 mM Ca^{2+}. Preliminary measurements show that *r*-EchAV and ANV have very similar phospholipid binding characteristics. The binding range between the two proteins and PS is approximately K_d = 1.83–2.15 nM, as shown in Fig. 3, *D–F*. At the same time, the binding of the two proteins to PC is much weaker than that of PS, and it is generally considered that there is no specific binding. Under the same conditions, BSA did not bind to PS or PC (data not shown). Based on the above findings (Fig. 3), it was shown that the activity of the ANV structure in the *r*-EchAV molecule was completely retained.

Tetrachoric assay of coagulation by r-EchAV

The activated partial thromboplastin time (aPTT) assays are useful in *in vitro* global tests for assessing the activities of the classical extrinsic, intrinsic, and common pathways of coagulation and for monitoring anticoagulant therapy. At the same concentration, the aPTT value prolonged by the *r*-EchAV group was slightly higher than that of the ANV group; *r*-EchAV was about 1.5-fold more potent than ANV, and both were significantly higher than the normal reference range (as shown in Fig. 4*A*). In terms of the effects on PT (plasma clotting time) value, FIB (fibrinogen) value, and TT (thrombin time) value, neither of them caused statistically significant changes; and they were all within the normal clinical reference range.

Furthermore, *r*-EchAV showed a dose-dependent effect on aPTT value (as shown in Fig. 4*B*). With the increase in the *r*-EchAV concentration, the aPTT value was significantly prolonged; and when the *r*-EchAV concentration was greater than 5 μmol/liter, the amplitude of aPTT changed more than the maximum within the normal reference range. However, when the concentration of *r*-EchAV increased, the PT value, FIB value, and TT value did not change much, and there was basically no statistically significant change.

The aPTT measures the intrinsic pathway activity, such as coagulation factors XII, XI, IX, and X, and the reduction in these coagulation factors will cause prolongation of the aPTT value. Based on the above analysis results, we speculate that *r*-EchAV cannot fully activate factor X by binding to Ca^{2+} and phospholipid molecules, thereby affecting the endogenous coagulation pathway and thus affecting the common coagulation pathway.

r-EchAV plasma coagulation time

The results are shown in Fig. 5; the turbidity dynamics of different plasma samples were measured using a microplate reader.

PS alone only weakly promotes plasma coagulation (Fig. 5*A*). This may be because PS binds to coagulant factors Xa and Va, which are involved in steps that are rather late in the coagulation cascade. As shown in Fig. 5*B*, when *r*-EchAV was added to plasma in a PS-coated well, the onset of coagulation was delayed; a concentration of 20 μM *r*-EchAV delayed the onset time of coagulation from 30 to 50 min. As the concentration of

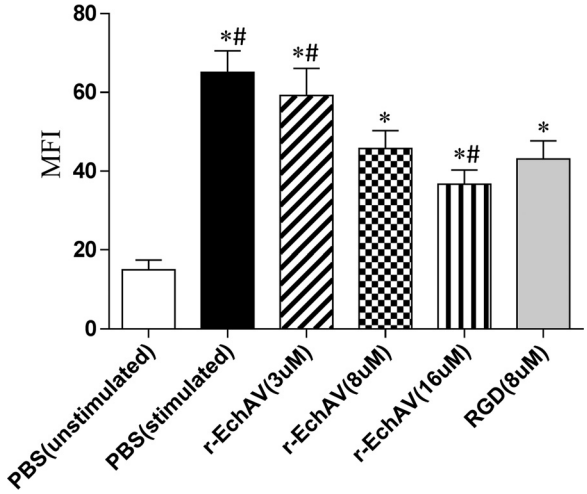

Figure 6. Quantitative alteration of mean fluorescence intensity of the $\alpha_{IIb}\beta_3$ receptor after exposure to various concentrations of *r*-EchAV by flow cytometry. * indicates significant difference compared with the unstimulated PBS as negative control ($p < 0.05$), and # means significantly different from the RGD sample as positive control ($p < 0.05$).

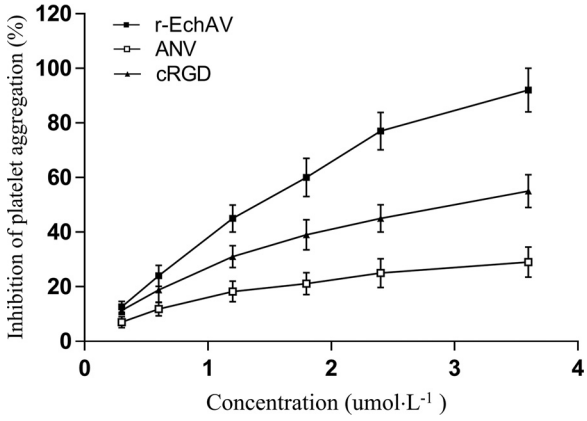

Figure 7. Antiplatelet aggregation activity of *r*-EchAV.

r-EchAV increased, the plasma clotting time was significantly prolonged. The delay effects of coagulation by *r*-EchAV were dose-dependent, but the effect was barely presented in a PC-coated well as compared with a PS-coated well. It is speculated that the combination of *r*-EchAV and PS can effectively prevent PS from participating in the activation of coagulation factor X in plasma, thereby reducing fibrin production, reducing plasma turbidity, and prolonging coagulation time. It is shown that *r*-EchAV can intervene in the coagulation process by binding to PS, thereby exhibiting a significant anticoagulant effect.

Whole-blood flow cytometry for detection of r-EchAV affinity for platelet $\alpha_{IIb}\beta_3$ receptors (25)

Previous studies have shown that there are a large number of activated integrin $\alpha_{IIb}\beta_3$ receptors on the surface of platelet cell membrane after ADP stimulation (18). A receptor binds to fibrinogen in plasma and plays an important role in platelet adhesion and aggregation. The $(\alpha_{IIb}\beta_3$ receptor/fibrinogen$)_n$ complex is also an important component of vascular emboli.

In the past, platelet glycoprotein research mostly used radioimmunoassay or platelet-rich plasma flow cytometry. In these methods, centrifugation, washing, and other processes can cause platelet activation and membrane glycoprotein destruction. The application of whole-blood flow cytometry can reduce the interference of human factors and simplify the experimental steps, making the experiment simple and fast. Therefore, we used whole-blood flow cytometry to detect the binding characteristics of *r*-EchAV to platelet $\alpha_{IIb}\beta_3$ receptors. The test results are shown in Fig. 6.

The results showed that the mean fluorescence intensity decreased with the increase in *r*-EchAV concentration and showed a dose-dependent effect. This indicates that *r*-EchAV significantly reduces the binding of fibrinogen to the activated platelet membrane, suggesting that *r*-EchAV can competitively bind to the activated platelet membrane $\alpha_{IIb}\beta_3$ receptor with fibrinogen.

Antiplatelet aggregation activity of fusion protein r-EchAV

Because of the special structure of *r*-EchAV, both ECH and ANV can interact with activated platelets, *i.e.* ECH binds to integrin receptor $\alpha_{IIb}\beta_3$ through its RGD functional motif, and ANV binds to PS exposed on the surface of activated platelets. We examined the effect of *r*-EchAV on ADP-stimulated platelet aggregation. The experimental results are shown in Fig. 7. Our studies have shown that *r*-EchAV can significantly inhibit the ADP-stimulated platelet aggregation and exhibit a dose-dependent effect. As the concentration of *r*-EchAV increases, the inhibitory effect is enhanced. By evaluating the aggregation–inhibition curve, we can determine that the IC_{50} of *r*-EchAV is about 1.5 μM, and the inhibition of activated platelet aggregation is more than 90% when the protein sample concentration reaches about 4 μM. Another interesting finding is that although ANV also exhibits a certain aggregation–inhibitory activity, the ability of *r*-EchAV is significantly higher than that of ANV. We speculate that this phenomenon is probably due to the full play of the biological function of ECH in the *r*-EchAV structure. However, the IC_{50} value of *r*-EchAV for platelet aggregation inhibition is lower than the reported IC_{50} value of recombinant ECH (320 nM) (26), which seems to imply that the steric hindrance produced by a significant increase in molecular weight has a negative effect on the interaction between the RGD domain of ECH and the integrin receptor $\alpha_{IIb}\beta_3$ on platelet membrane. However, this negative effect due to steric hindrance is compensated to some extent by the interaction of the ANV domain on *r*-EchAV with a large number of exposed PS molecules on the activated platelet membrane (as shown in Fig. 8). Therefore, we speculate that the inhibitory effect of *r*-EchAV on aggregation of activated platelets may be the result of the combination of the above two effects.

Effect of r-EchAV on mouse tail-bleeding times

The concentration of the *r*-EchAV administered to mice *in vivo* was 0.01 μmol/kg. Compared with the saline group, the bleeding time of the *r*-EchAV experimental group was significantly different ($p < 0.01$, two-tailed unpaired *t* test with Welch correction). As the protein concentration of *r*-EchAV increased, the bleeding time was significantly prolonged, and the risk of bleeding increased. When the concentration of the sample protein *r*-EchAV was increased by 3.9 times, the bleeding time was longer than that of the heparin group (200 μmol/

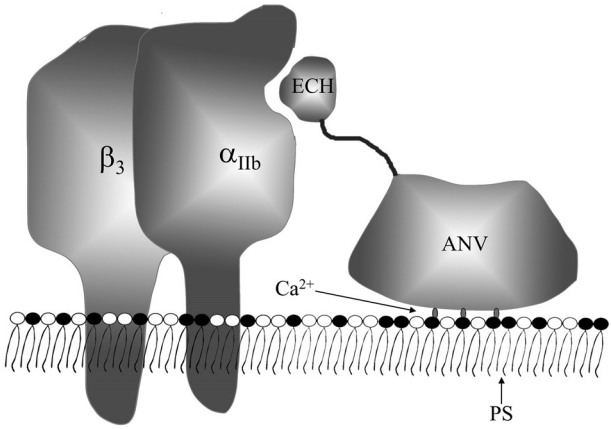

Figure 8. Model of the inhibition of a membrane-associated coagulation by the *r*-EchAV based on the double anchor mechanism to PS and $\alpha_{IIb}\beta_3$. The fusion protein binds to PS on the membrane surface in a Ca^{2+}-dependent manner via the ANV domain. This facilitates the binding of the ECH to the active site of the integrin $\alpha_{IIb}\beta_3$ receptor.

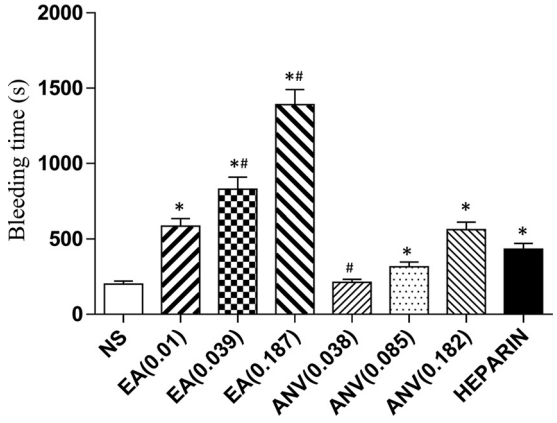

Figure 9. Bleeding time in *r*-EchAV mice. * indicates a significant difference compared with the saline group ($p < 0.05$), and # means significantly different from the heparin group ($p < 0.05$).

kg), and the difference was significant ($p < 0.01$, paired two-tailed *t* test). The bleeding time in the ANV group was 193 s at 0.038 μmol/kg, 289 s at 0.085 μmol/kg, and 1142 s at 0.2 μmol/kg, respectively (Fig. 9). Compared with ANV alone, the *in vivo* bleeding time of *r*-EchAV was significantly prolonged, indicating that the *in vivo* activity of *r*-EchAV was stronger than that of ANV alone.

Discussion

Thrombotic diseases are characterized by high morbidity, disability, and mortality, which seriously endanger human life and health. The prevention and treatment of thrombosis have attracted much attention. The development and use of anticoagulant drugs are still hot topics in medical research today. The mechanism of thrombosis is complex, in which platelets and coagulation systems are more important factors. At present, antithrombotic and anticoagulant drugs for clinical application are of great significance for the prevention and treatment of thrombotic diseases by antagonizing different coagulation factors and inhibiting pathological embolism.

The anionic phospholipid PS is located in the inner leaflet of the plasma membrane in normal healthy cells. Upon injury, activation, or apoptosis, PS is actively externalized to the outer leaflet of the plasma membrane and sheds microparticles, which are procoagulant. Coagulation is initiated by formation of a tissue factor/factor VIIa complex on PS-exposed membranes and propagated through the assembly of intrinsic tenase (factor VIIIa/factor IXa), prothrombinase (factor Va/factor Xa), and factor XIa complexes on PS-exposed activated platelets. Targeted drug delivery (TDD), a strategy that is intended to treat disease effectively with minimal detrimental side effects, is based on the principle of Paul Ehrlic's "Magic Bullet," namely it is a therapeutic compound that is guided to the diseased lesion by a targeting function. The targeting function can be an integral part of the therapeutic compound or can be deliberately attached to the drug (27). Cell surface–expressed PS is potentially an attractive target for TDD, especially for the prevention and treatment of platelet-derived thrombosis. ANV is a human protein that binds with high affinity and specificity to the abundant PS molecules exposed on activated platelets and accumulates selectively in thrombi after intravenous administration in animal models of arterial thrombosis (28).

ANV is often used as a guiding molecule for targeting PS to construct potential recombinant protein drug candidates for the treatment of thrombotic diseases. It has been reported that in the animal arterial embolization model, the radionuclide-labeled ANV concentrated in the thrombus of the animal model was 13 times higher than in the control group (29). Thiagarajan and Tait (16) found that when platelets were activated by thrombin and collagen, the binding site of ANV to platelets increased 15–20 times, and ANV was also found to inhibit platelet binding to factor Xa. Tait *et al.* (28) studied the biodistribution and thrombus binding of ANV in rabbit and swine models of fully occlusive arterial thrombi and indicated that ANV is useful as an agent for selective targeting of platelet-containing thrombi. The capacity of ANV to bind calcium-dependently to PS has led to the proposal that ANV plays a role in the antithrombotic arm of blood coagulation (11, 30). Platelet-expressed PS supports the assembly of the prothrombinase complex composed of factor Va (FVa), factor Xa (FXa), and prothrombin (31). The prothrombinase complex subsequently converts the zymogen prothrombin into proteolytically active thrombin (32). Thrombin in turn converts fibrinogen into fibrin polymers that stabilize the platelet plug on the damaged vessel wall (33). ANV competes with FVa, FXa, and prothrombin for binding to PS, thereby preventing the formation of the prothrombinase complex and, consequently, the formation of thrombin (34). In solution, ANV is present as a monomer, but once bound to PS-expressing membrane, three monomers build a trimer via protein–protein interactions, and the trimers assemble into a two-dimensional lattice covering the PS expressing surface by trimer–trimer interactions (35, 36). Alternatively, it was proposed that ANV inhibits thrombin generation by forming a two-dimensional lattice on the PS-expressing surface (37).

Two chimeras were designed: prourokinase(1–411)–ANV(1–320) and prourokinase(144–411)–ANV(1–320) (amino acid numbers of parent proteins are given in parentheses) (38). This study showed the feasibility of hybrid thrombolytic agents in which ANV provides the platelet-containing thrombi-targeting component. A 1:1 stoichiometric conjugate of ANV and the

B-chain of urokinase connected by a disulfide bond has previously been reported, and the data from this study once again support the argument that ANV is a useful agent for targeting plasminogen activators to phospholipid-containing thrombi (39). A recombinant human ANV–hirudin chimeric protein was shown to have dose-dependent thrombin inhibitory activity (40). Four recombinant fusion proteins (ANV–KPIs) were constructed by linking ANV to the Kunitz-type protease inhibitor (KPI) domain of tick anticoagulant protein, an aprotinin mutant (6L15), β-amyloid protein precursor, or tissue factor pathway inhibitor (41). Through *in vitro* and *in vivo* experiments, the authors suggested that ANV–KPI proteins represent a new class of anticoagulants that specifically target the anionic membrane-associated coagulation enzyme complexes present at sites of thrombogenesis. It is of considerable interest to explore the therapeutic use of these proteins in the prevention and treatment of thrombosis associated with many other pathological states. A chimeric protein consisting of the extracellular domain of tissue factor (soluble TF or sTF) and ANV was constructed, and both the sTF and ANV domains had ligand-binding activities consistent with their native counterparts (42). Interestingly, the chimera exhibited biphasic effects upon blood coagulation. Specifically, it accelerated blood coagulation at a low concentration, whereas at higher concentrations, it acted as an anticoagulant. The sTF–ANV chimera is regarded as a targeted procoagulant protein that may be useful in accelerating thrombin generation where PS is exposed to the vasculature. DAV (73 kDa), a homodimer of human ANV, was constructed and exhibited a higher affinity for PS-exposing cells than ANV (43). DAV was found to be a potent inhibitor of the activity of the prothombinase complexes and reduced the formation of mediators of blood coagulation and reperfusion injury. DAV is considered to be a valuable probe to measure PS exposure and may be efficacious as a novel drug in clinical situations.

In this study, human ANV was fused to ECH, a potent antiplatelet polypeptide derived from snake venom. The C terminus of ECH was linked to the N terminus of ANV via a tetraglycine linker (Figs. 1 and 8). It is well-known that the ECH polypeptide belongs to the disintegrin family, which is characterized by strong integrin receptor recognition and binding ability. Therefore, in many physiological and pathological phenomena involving integrin receptors, the integrin family is generally capable of showing strong antagonistic characteristics. Because the integrin receptor family has a large number of members, each has its own distribution characteristics and participates in different physiological and pathological activities. Therefore, different disintegrins often exhibit different integrin receptor-binding characteristics and thus manifest in different physiological and pathological phenomena. ECH is a disintegrin derived from viper snake venom (44) without post-translational modifications. ECH strongly antagonizes platelet aggregation and has a high affinity and binding to the integrin receptor $\alpha_{IIb}\beta_3$, which is abundant in activated platelets and plays an important role in thrombosis. Platelet $\alpha_{IIb}\beta_3$ integrin blockade appears to be instrumental in improving clinical outcomes following percutaneous intervention, with clinical benefit extending to all patient categories (45). The findings in IMPACT II and EPILOG suggest that the entire spectrum of patients who undergo coronary intervention benefit from $\alpha_{IIb}\beta_3$ blockade. Clinical evaluation of the antiplatelet glycoprotein $\alpha_{IIb}\beta_3$ receptor antagonists has now extended over nearly a decade. The largest experience to date with this new class of agents has been in the prevention and management of complications of percutaneous coronary intervention (46, 47). The RGD motif in ECH plays a crucial role in its binding to the $\alpha_{IIb}\beta_3$ receptor. However, naturally extracted ECH is difficult to obtain, even through the purchase method. Regarding the preparation of recombinant ECH, we have not yet established it nor can we obtain external donations of recombinant ECH products for the time being. It has been reported that a cyclic RGD-containing decapeptide, cyclo-(*S*,*S*)-GCARGDWPCA in which two cysteine residues are linked as disulfide bond, has a relatively potent antiplatelet aggregation effect (48). Therefore, we synthesized and further used this RGD-cyclic decapeptide instead of the ECH as a positive control to detect the inhibition of human platelet aggregation by *r*-EchAV recombinant protein under the same conditions. The detailed investigation results indicated that for ADP-stimulated platelet aggregation, *r*-EchAV showed a high degree of antagonism, and its platelet aggregation–inhibitory activity (IC_{50} = 1.5 μM) was higher than that of the RGD-cyclic polypeptide (IC_{50} = 3 μM) as a positive control, and it was also significantly higher than that of ANV (low activity, no exact IC_{50} value). The results of flow cytometry also indicated that the *r*-EchAV molecule exhibited significant $\alpha_{IIb}\beta_3$ receptor affinity. These are closely related to the effective binding of $\alpha_{IIb}\beta_3$ to the ECH domain in the *r*-EchAV molecule. Although the antiplatelet aggregation activity of ECH alone is very high, there are currently no reports and experiments using ECH in clinical treatment. We believe that the use of ECH alone is not clinically feasible. The reasons are as follows. As a polypeptide extracted from the snake venom of the saw-scaled viper *Echis carinatus* species, the extreme scarcity of snake venom resources determines that it is unlikely that the extracted natural ECH will be directly used as a therapeutic drug for a wide range of clinical applications. A very limited number of echistatins obtained from the extraction are also used only in scientific research in some laboratories. Natural ECH extracts may also be contaminated with other traces of unidentified impurities in snake venom, which may pose a potential threat to the human body. Although there are reports on the preparation of recombinant ECH by recombinant DNA technology, there has not been a truly meaningful increase in yield, and recombinant ECH is currently difficult to purchase directly. At present, there is no report on the stability, pharmacokinetics, and side effects of recombinant ECH. Recombinant ECH has not been reported in clinical practice. Therefore, in the inhibition of antiplatelet aggregation, the *r*-EchAV is less active than ECH alone, but this should not pose a serious threat to the possible application of *r*-EchAV in the future. *r*-EchAV can bind to Ca^{2+} and PS, so that factor X cannot be fully activated and exerts an anticoagulant effect by acting on endogenous coagulation pathway; this ability should be attributed to the ANV domain in the *r*-EchAV molecule. In summary, for plasma clotting time *in vitro*, *r*-EchAV was also higher than that of ANV alone. As the concentration of *r*-EchAV increased, the plasma clotting time was significantly prolonged and showed a dose-dependent effect. Compared with the ANV molecule

alone, the bleeding time *in vivo* of the animal model of *r*-EchAV also showed a significant prolongation, indicating that the anticoagulant activity of *r*-EchAV was better than that of individual ANV.

r-EchAV, which combines two commonly recognized anticoagulation mechanisms, showed good targeting to platelet-rich thrombi and exhibited good anticoagulant and antithrombotic effects *in vivo*. *r*-EchAV is very suitable as a new drug candidate for antithrombotic TDD strategy. In addition, *r*-EchAV exhibits good water solubility characteristics. During preparation, *r*-EchAV was present in a soluble state. Good solubility is very beneficial for the possible clinical therapeutic use of *r*-EchAV in the future.

Our study showed that the active structures of ANV and ECH were well retained in the *r*-EchAV molecule. The intact ANV moiety maintains the stability of the overall fusion protein molecule. This benefit is also reflected in the preparation of the *r*-EchAV fusion protein, which can better maintain the stability of the *r*-EchAV molecule and allow for efficient purification and preparation of recombinant *r*-EchAV. However, we do not have to extract *r*-EchAV from the inclusion bodies produced by bacteria compared with the previous technique for preparing ANV. This avoids complicated and cumbersome protein denaturation–renaturation steps, which facilitate the simplification of the preparation process and maintains the integrity and biological activity of the recombinant protein structure. The reliability of its production is very important for the possible therapeutic application and development of *r*-EchAV in the future.

Experimental procedures

Materials

E. coli DH5α used for plasmid amplification was purchased from Invitrogen (Beijing, China), and *E. coli* BL21 (DE3) used for the expression of the fusion protein was purchased from Novagen (Beijing, China). *E. coli* BL21 (DE3) is a λ lysogen of *E. coli* BL21 wherein the prophage contains the RNA polymerase gene of T7 bacteriophage under the control of the *lac* UV5 promoter (49). Plasmid pJET1.2/blunt vector was purchased from ThermoFisher Scientific (Shanghai, China). Plasmid pGEX-6P-1, a vector for producing fusion protein with the GST (50), was purchased from GE Healthcare (Beijing, China). *E. coli* DH5 and BL21 (DE3) strains were grown at 37 °C in Luria-Bertani (LB) medium with (100 μg/ml) or without ampicillin (51). ANV, bovine fibrinogen, PS (bovine brain), and PC (bovine brain) were from Sigma. IPTG was purchased from Promega (Madison, WI). The mouse anti-ANV polyclonal antibody was purchased from Abcam Co. Ltd. The RGD-containing peptide (cyclo-*S,S*-(GCGRGDWPCA)) was synthesized by Beijing Jinsheng Biotech Co., Ltd. Sephacryl S200HR gel and GST affinity medium were purchased from GE Healthcare; FITC-labeled goat anti-human fibrinogen was purchased from Beijing Noble Technology Co., Ltd. Coomassie Brilliant Blue G-250, R-250, Goldview, glycine, TEMED, ampicillin, tetramethylbenzidine, diaminobenzidine, skim milk powder, HRP goat anti-mouse IgG secondary antibody, ADP·Na_2, etc., were purchased from Beijing Dingguo Changsheng Biotech Co., Ltd. Ultrafiltration tubes (3, 10, and 30 kDa) were purchased from Merck-Millipore (Beijing, China). Human blood was acquired from a healthy male donor who had not taken any aspirin or similar medication for at least 2 weeks after informed consent. The study has been approved by the Biomedical Ethics Committee of Beijing Normal University and was performed according to the principles outlined in the Declaration of Helsinki.

Cloning and synthesis of cDNA for ANV and ECH

The ORF of human ANV was cloned by RT-PCR and sequenced. ANV cDNA was generated from human placental mRNA by PCR using ANV reverse primer 1 and forward primer 2 (Table 1*A*) (23). We extracted total RNA from human placenta by the standard guanidinium thiocyanate procedure and used primers (ANV reverse primer 1 and forward primer 2) based on EMBL/GenBank/DDBJ accession number J03745 with BamHI and XhoI sites. Human ANV cDNA was cloned and finally ligated between BamHI/XhoI sites at multicloning sites of the plasmid pGEX-6P (Amersham Biosciences) for expression in *E. coli* as a GST–ANV fusion protein.

The DNA fragments containing the ORF of ECH was created by PCR using oligonucleotide-directed mutagenesis. Specifically, primary amplification was performed using E1F and E1R as templates, and on the basis of this, E2F and E2R primers were used for secondary DNA amplification. The DNA product produced in the reaction system was identified by electrophoresis, and the corresponding DNA fragment was purified and recovered. The correctness of the nucleotide sequence of the constructed recombinant ECH gene was verified by DNA sequencing.

Construction of the r-EchAV gene

ECH cDNA, lacking a stop codon for the purpose of creating fusion molecules, was generated based on whole-length ORF of synthetic ECH by PCR using E3F and E3R primers, ANV reverse primer 1, and forward primer 2 (Table 1A).

Using the constructed pGEX-6P-1–ANV recombinant plasmid as a template, using E3F and E3R primers, 10 μl of 5× buffer (containing Mg^{2+}), 5 μl of dNTP mix, 1 μl of DNA polymerase, and finally 29 μl of distilled water were added to make up a 50-μl PCR amplification reaction system.

The PCR conditions were set as follows: predenaturation at 95 °C for 5 min, denaturation at 95 °C for 1 min, annealing at 56 °C for 1 min, extension at 72 °C for 2 min (30 cycles), and final extension at 72 °C for 10 min. The reaction product was stored at 4 °C.

The DNA fragments produced by the above two DNA amplification systems were purified, identified, and then mixed, and a new DNA amplification system was constructed using E3F and LAA-3 primers. By purifying and recovering the DNA product, a DNA-amplified fragment of 1226 bp in length was finally obtained. Furthermore, the amplified product was subjected to DNA sequencing determination and aligned with the expected base sequence of *r*-EchAV to finally confirm the correctness of the *r*-EchAV gene construct.

Recombinant plasmids were transfected into *E. coli* DH5α for cloning and selection. The confirmed synthetic *r*-EchAV

gene was cloned into pJET1.2/blunt vector and transferred into *E. coli* DH5α and further subcloned into plasmid pGEX-6P-1 at the sites of BamHI and XhoI for expression in *E. coli* (DE3) as a GST-coupled fusion protein.

Expression of r-EchAV fusion protein in E. coli

A total of 10 ml of an overnight culture was inoculated into 1 liter of TM medium containing 50 μg/ml ampicillin and maintained at 37 °C until the optical density at 600 nm (OD_{600}) of the culture reached 0.5. The culture was induced by adding IPTG to a final concentration of 100 μM and continuously shaking at 25 °C for 12 h. We explored the optimum quantity of IPTG as the inducer, the optimum temperature, and the time of IPTG induction, and we finally determined the optimum induction conditions. The cells were harvested by centrifugation at 6000 × *g* at 4 °C for 15 min, and the cell pellet was frozen at −80 °C for further use. The pellet was washed and resuspended in 20 ml of cold phosphate-buffered saline (PBS, 140 mM NaCl, 2.7 mM KCl, 10 mM Na_2HPO_4, 1.8 mM KH_2PO_4, pH 7.3). The cells were lysed by sonication, and a final concentration of 1 mg/ml lysozyme, 5 μg/ml DNase I, 5 μg/ml RNase, and 1% (v/v) of Triton X-100 was added. After incubation on ice for 15 min and centrifugation at 12,000 × *g* for 20 min at 4 °C, the lysate of cells containing the soluble fraction and the cell debris was separated and analyzed by 12% sodium lauryl sulfate-PAGE (SLS-PAGE) at 100 V using a Mini-protein system (Bio-Rad, Beijing, China) and stained with Coomassie Brilliant Blue R-250 (52).

Preparation of ANV and r-EchAV coupled with GST by binding and elution from affinity chromatography

The supernatant containing the GST–ANV (from construct pGEX–*rh*-AV) or fusion protein or GST–*r*-EchAV (from construct pGEX–*r*-EchAV) was filtered through a cellulose acetate filtration membrane with 0.45-μm pores and then passed through an affinity chromatography column of GSH-Sepharose 4B (Amersham Biosciences) equilibrated with 1× PBST (PBS + 1% Triton X-100) with the flow rate of 0.5 ml/min. To remove any contaminating proteins, the column was washed with about seven bed volume of PBS with the flow rate of 1.0 ml/min until the UV detector count dropped to baseline. The recombinant fusion proteins were then eluted out with 10 ml of 50 mM Tris-HCl buffer containing 10 mM reduced GSH, pH 8.0. The fusion protein-containing fractions were pooled and concentrated using Centricon Microconcentrators (Millipore, Beijing, China) with a 10-kDa molecular mass cutoff and centrifuged at 3000 × *g* for 10 min at 4 °C, and reduced GSH was removed; the concentrate was diluted with 1× PBS and ultrafiltered again. The collection of protein concentrate was evaluated by SLS-PAGE. The protein concentration was determined by the method of Bradford using BSA as a protein standard (53). The column was washed with a 2× volume of 0.5 M NaOH solution to remove nonspecifically adsorbed impurities, washed with double-distilled H_2O to neutrality, and finally washed with a 4× volume of 20% ethanol and stored at 4 °C.

Cleavage and purification of r-EchAV fusion protein

For site-specific protease cleavage, *r*-EchAV fusion protein was incubated with PSP™ protease (1000 units/mg, Nantong Baoyuan Biotech Ltd., China) at a molar ratio of 800:1 (M/M) in lysis buffer (0.5 M Tris-HCl + 150 mM NaCl + 0.1% Triton X-100, pH 8.0) at 4 °C for 12 h. For PSP™ protease cleavage, various conditions were tested. The above was found to be the optimum molecular molar ratio of the substrate/enzyme. The PSP protease contains a GST domain. To remove the GST and the PSP protease, the reaction mixture was passed through a GSH-Sepharose 4B column (Amersham Biosciences, Beijing, China) that could specifically bind to the digested product GST and the PSP™ protease containing the GST domain with a flow rate maintained at 1 ml/min at 4 °C. The eluate containing the target protein component was collected and subjected to concentration and desalting by 10-kDa Millipore ultrafiltration. The elution and the PSP™ protease reaction were analyzed by 12% SLS-PAGE at 100 V and stained with Coomassie Brilliant Blue R-250.

Protein determination

The protein concentration was determined by the method of Bradford using BSA as a protein standard (53).

The purified ANV protein and the *r*-EchAV fusion protein were subjected to Western blot analysis; the primary antibody was an anti-ANV polyclonal antibody, and the secondary antibody was an HRP goat anti-mouse antibody.

The SEC-HPLC profile of *r*-EchAV fusion protein was carried out further by means of SEC-HPLC L260U (Agilent Technologies, Beijing, China) with Sephacryl S200 gel column. First, the quaternary pump and detectors of the SEC-HPLC were turned on and self-tested, setting the parameter of the flow rate $v = 5$ ml/min, washing ~2 volumes of the column with water to remove air bubbles. Second, the HPLC system was equilibrated with 1× PBS for ~2 column volumes until the baseline was stable, and 200 μl of the *r*-EchAV fusion protein was loaded and injected in 1 column volume of 1× PBS, and finally, the column and pipes were washed with ultrapure water and 10% methanol, respectively, and the elution spectra were recorded and analyzed. All materials or solutions, including ultrapure water, an equilibration solution (1 × PBS), the purified *r*-EchAV fusion protein–containing solution, and 10% methanol, must be filtered through a 0.22-μm needle-shaped filter before loading onto the HPLC system.

Phospholipid-binding assay of r-EchAV

A total of 10 mg of PS or PC was dissolved in 10 ml of chloroform, added to each microtiter well (2.5 μg/well), and adsorbed onto the polystyrene surface by evaporating off the solvent at 37 °C. The plate was blocked with 5% skim milk in Tris-buffered saline (TBS) for 2 h at 37 °C. Protein samples such as *r*-EchAV fusion protein at various concentrations were added to the wells, followed by incubation for 2 h in the presence of 5 mM $CaCl_2$. The wells were then washed with TBS containing 1 mM $CaCl_2$ three times and blocked with 2% skim milk for 1 h. Mouse antirecombinant human ANV polyclonal antibodies, which were prepared in our laboratory (23), were added to the wells and incubated for 1 h. The wells were then

washed and blocked with 2% skim milk for 15 min. HRP-labeled goat anti-mouse IgG was added to the wells, and then the plate was incubated for 60 min. The wells were then washed and developed by the addition of 140 μl of 0.03% (w/v) tetramethylbenzidine and 0.018% (v/v) H_2O_2 in citrate/acetate buffer, pH 5.0. Color development was stopped by the addition of 40 μl of 2 N H_2SO_4. The absorbance of each well was then read at 450 nm.

Phospholipid binding dose analysis was carried out as follows. The amount and concentration in each well of *r*-EchAV were 50 μl and 50 μg/ml, respectively. The doses of PS were set to 0, 0.4, 0.8, 1.2, 1.6, 2.0, 2.4, 2.8, and 3.2 μg, and the other steps were the same as above.

The effect of calcium ion concentration on *r*-EchAV binding to phospholipids was carried out as follows. The amount and concentration in each well of *r*-EchAV were 50 μl and 50 μg/ml, respectively. The PS dose was set to 2.5 μg, and the Ca^{2+} concentration in the binding buffer was set to 0, 0.01, 0.05, 0.1, 0.5, 1.0, 3, 5, 10, 20, 50, and 100 mM. The other steps were the same as above.

Surface plasmon resonance (SPR) (54)

The SPR measurements were conducted on a BI-SPR 4000 system (Biosensing Instrument Inc., Tempe, AZ). Running buffer was degassed under a vacuum for 40 min. Samples were preloaded into a 200-μl sample loop and then injected to the flow cell by a syringe pump (model 260, KD Scientific, Holliston, MA) at a flow rate of 10 μl/min. A 100% PC bilayer was immobilized onto the control flow cell. The cells were regenerated with 5 mM EDTA in HBS (10 mM Hepes, 150 mM NaCl, pH7.4) between each cycle. The chip was an L1 biosensor chip. The dilution buffer for ANV or *r*-EchAV was 10 mM Hepes + 150 mM NaCl + 2 mM $CaCl_2$. The temperature was 25 °C.

Plasma coagulation assay

A total of 2.5 μg of PS or PC (chloroform as a solvent) was added to each microtiter well and then adsorbed by evaporating off the solvent at 37 °C. The plate was blocked with 5% skim milk powder in TBS at 37 °C for 2 h and washed three times by washing buffer. The *r*-EchAV was diluted in the binding buffer to different concentrations, and then 50 μl of each protein dilution was added to each well, incubated at 37 °C for 2 h, and washed three times. 100 μl of 50% plasma (PBS as the solvent) was prepared and added to each well, and incubation was carried out for 3 min at 37 °C. 25 μl of 0.08 M $CaCl_2$ (final concentration, 15 mM) was added to each well, and the plasma began to coagulate. The absorbance of each well was read at 405 nm and measured every 5 min. The onset time of fibrin formation in the analysis was defined as the time when the absorbance value in each well was elevated by more than 0.1 above the baseline.

Blood-clotting tetrachoric assay

Pooled normal plasma, anticoagulated with 1:9 dilution of 3.8% citrate, was stored at −80 °C until use. All reagents were prewarmed to 37 °C, and assays were performed in triplicate. Human whole blood was centrifuged at 3000 rpm for 10 min, and the supernatant was taken as platelet-poor plasma (PPP). Then, 300 μl of PPP and 30 μl of protein sample (PBS as control) were added to each assay cup, and the mixture was incubated at 37 °C for 10 min. Finally, the aPTT, PT, TT, and FIB assays were carried out on a CS-5100 coagulation analyzer (Sysmex Co. Ltd., Japan).

Platelet aggregation assay

Human blood was collected in a 3.8% sodium citrate solution (1:9) from healthy volunteers who had not taken any aspirin or related medication for at least 2 weeks. PRP was obtained by centrifugation at 800 rpm for 10 min, and a second centrifugation at 3500 rpm for 15 min was used to prepare PPP. The PRP was diluted with the PPP to a platelet count of 450,000/μl. Three hundred microliters of PRP was added to a colorimetric cup, and then 30 μl of protein sample was added. There were three kinds of protein samples with different concentrations: *r*-EchAV, ANV, and RGD peptides. The colorimetric cups were incubated at 37 °C for 5 min, and ADP (final concentration, 10 μM) was used to induce platelet aggregation. The extent of the inhibition of platelet aggregation was assessed by comparison with the maximal aggregation induced by the control dose of agonist (10 mM ADP). The IC_{50} value was determined from the increasing concentration curves. All experiments were performed in triplicate.

$\alpha_{IIb}\beta_3$ receptor affinity analysis of r-EchAV (55)

One milliliter of human whole blood was collected with a sodium citrate anticoagulation tube and, within 4 h, was centrifuged at 800 rpm for 8 min at room temperature. The supernatant was PRP. The samples were added in the following order: PRP 5 μl, sample to be tested (including *r*-EchAV, or PBS, or RGD peptide) 5 μl, ADP 5 μl, and then PBS 35 μl. The final volume of the liquid in each tube was 50 μl, and it was mixed gently and incubated for 10 min at room temperature. The final concentration of ADP was 2 μM. Next, 450 μl of 4% paraformaldehyde was added to each tube, and immobilization at room temperature was conducted for 45 min. Then, 5 μl of FITC-labeled goat anti-human fibrinogen antibody was added to each tube and incubated at 37 °C for 30 min. In the flow cytometry test by means of a FACSCalibur™ flow cytometer (BD Biosciences), the excitation wavelength was set to 488 nm, and the fluorescence intensity was measured. Data acquisition was triggered by forward light scatter with all photomultipliers in the log mode. Noise was reduced during analysis by eliminating events with forward and side scatter values different from those characteristics of the lipospheres. Mean log fluorescence was converted to linear fluorescence for the values depicted in the figures. Only experiments in which the fluorescence histogram indicated a log-normal distribution, as judged by inspection, were analyzed quantitatively. Flow cytometry experiments were performed in 0.14 M NaCl, 0.02 M Tris-HCl, 1.5 or 5 mM $CaCl_2$ as indicated in figure legends, and 0.1% bovine albumin, pH 7.5. The experiment was repeated three times.

Assay for in vivo bleeding time in mice

KM mice (male 25 ± 1 g body weight, 5 weeks old) were obtained from Beijing Vital River Laboratory Animal Technology Co., Ltd. Mice were housed in accordance with and studied using a protocol approved by the Animal Care and Use Com-

mittee of Beijing Normal University, College of Life Sciences. Bleeding time in the mice was measured by the method described by Dejana *et al.* (56). Anesthesia was performed by intraperitoneal injection of 1% sodium pentobarbital 0.1 ml, and the posterior venous plexus was injected with the test sample. A cut of 6 mm from the tail of the mouse was done 20 min after the injection. Bleeding time was recorded from the beginning of bleeding to its end. *r*-EchAV doses were adopted with 0.01, 0.039, and 0.187 μmol/kg (the solvent was normal saline), respectively. The normal positive control group was heparin sodium solution (heparin) at a dose of 200 units/kg. A two-tailed, paired *t* test was used to compare the two bleeding times. All proteins were injected in amounts equimolar with the *r*-EchAV fusion ones.

Statistical analysis

Data are expressed as the mean ± S.D. Student's *t* test or one-way analysis of variance were used to test for differences between two groups or three or more groups, respectively. $p < 0.05$ was deemed statistically significant.

Author contributions—J. J. conceptualization; J. J. resources; J. J. and Y. S. data curation; J. J. and Y. S. formal analysis; J. J. supervision; J. J. funding acquisition; J. J. and Y. S. validation; J. J. and Y. S. investigation; J. J. and Y. S. methodology; J. J. writing-original draft; J. J. project administration; J. J. writing-review and editing.

Acknowledgments—We thank Professor Qun Wei (Beijing Normal University) for advice on this work and Professor Tianwei Jing and Xigang Liu (Biosensing Instrument Inc.) for providing support in SPR analysis.

References

1. Vorchheimer, D. A., and Becker, R. (2006) Platelets in atherothrombosis. *Mayo Clin. Proc.* **81,** 59–68 CrossRef Medline
2. Wolf, P. (1967) The nature and significance of platelet products in human plasma. *Br. J. Haematol.* **13,** 269–288 Medline
3. Heemskerk, J. W., Bevers, E. M., and Lindhout, T. (2002) Platelet activation and blood coagulation. *Thromb. Haemost.* **88,** 186–193 CrossRef Medline
4. Verlinden, N. J., Coons, J. C., Iasella, C. J., and Kane-Gill, S. L. (2017) Triple antithrombotic therapy with aspirin, P2Y12 inhibitor, and warfarin after percutaneous coronary intervention: an evaluation of prasugrel or ticagrelor versus clopidogrel. *J. Cardiovasc. Pharmacol. Ther.* **22,** 546–551 CrossRef Medline
5. Cannon, C. P., Bhatt, D. L., Oldgren, J., Lip, G. Y. H., Ellis, S. G., Kimura, T., Maeng, M., Merkely, B., Zeymer, U., Gropper, S., Nordaby, M., Kleine, E., Harper, R., Manassie, J., Januzzi, J. L., *et al.* (2017) Dual antithrombotic therapy with dabigatran after PCI in atrial fibrillation. *N. Engl. J. Med.* **377,** 1513–1524 CrossRef Medline
6. Vance, J. E., and Steenbergen, R. (2005) Metabolism and functions of phosphatidylserine. *Prog. Lipid. Res.* **44,** 207–234 CrossRef Medline
7. Choo, H. J., Kholmukhamedov, A., Zhou, C., and Jobe, S. (2017) Inner mitochondrial membrane disruption links apoptotic and agonist-initiated phosphatidylserine externalization in platelets. *Arterioscler. Thromb. Vasc. Biol.* **37,** 1503–1512 CrossRef Medline
8. Obydennyy, S. I., Sveshnikova, A. N., Ataullakhanov, F. I., and Panteleev, M. A. (2016) Dynamics of calcium spiking, mitochondrial collapse and phosphatidylserine exposure in platelet subpopulations during activation. *J. Thromb. Haemost.* **14,** 1867–1881 CrossRef Medline
9. Nagata, S., Suzuki, J., Segawa, K., and Fujii, T. (2016) Exposure of phosphatidylserine on the cell surface. *Cell Death Differ.* **23,** 952–961 CrossRef Medline
10. Zhao, L., Wu, X., Si, Y., Yao, Z., Dong, Z., Novakovic, V. A., Guo, L., Tong, D., Chen, H., Bi, Y., Kou, J., Shi, H., Tian, Y., Hu, S., Zhou, J., and Shi, J. (2017) Increased blood cell phosphatidylserine exposure and circulating microparticles contribute to procoagulant activity after carotid artery stenting. *J. Neurosurg.* **127,** 1041–1054 Medline
11. Reutelingsperger, C. P., Hornstra, G., and Hemker, H. C. (1985) Isolation and partial purification of a novel anticoagulant from arteries of human umbilical cord. *Eur. J. Biochem.* **151,** 625–629 CrossRef Medline
12. Raynal, P., and Pollard, H. B. (1994) Annexins: the problem of assessing the biological role for a gene family of multifunctional calcium- and phospholipid-binding proteins. *Biochim. Biophys. Acta* **1197,** 63–93 CrossRef Medline
13. Huber, R., Römisch, J., and Paques, E. P. (1990) The crystal and molecular structure of human annexin V, an anticoagulant protein that binds to calcium and membranes. *EMBO J.* **9,** 3867–3874 CrossRef Medline
14. Voges, D., Berendes, R., Burger, A., Demange, P., Baumeister, W., and Huber, R. (1994) Three-dimensional structure of membrane-bound annexin V. A correlative electron microscopy-X-ray crystallography study. *J. Mol. Biol.* **238,** 199–213 CrossRef Medline
15. Lewit-Bentley, A., Morera, S., Huber, R., and Bodo, G. (1992) The effect of metal binding on the structure of annexin V and implications for membrane binding. *Eur. J. Biochem.* **210,** 73–77 CrossRef Medline
16. Thiagarajan, P., and Tait, J. F. (1990) Binding of annexin V/placental anticoagulant protein I to platelets. Evidence for phosphatidylserine exposure in the procoagulant response of activated platelets. *J. Biol. Chem.* **265,** 17420–17423 Medline
17. Thiagarajan, P., and Tait, J. F. (1991) Collagen-induced exposure of anionic phospholipid in platelets and platelet-derived microparticles. *J. Biol. Chem.* **266,** 24302–24307 Medline
18. Shattil, S. J., Hoxie, J. A., Cunningham, M., and Brass, L. F. (1985) Changes in the platelet membrane glycoprotein IIb. IIIa complex during platelet activation. *J. Biol. Chem.* **260,** 11107–11114 Medline
19. Shi, J., and Gilbert, G. E. (2003) Lactadherin inhibits enzyme complexes of blood coagulation by competing for phospholipid-binding sites. *Blood* **101,** 2628–2636 CrossRef Medline
20. Uchman, B., and Triplett, D. A. (2015) Inhibition of binding of β2-glycoprotein 1 to phosphatidylserine by polymyxin B, a lupus-like anticoagulant. *Clin. Appl. Thromb. Hemost.* **21,** 584–585 CrossRef Medline
21. Marder, L. S., Lunardi, J., Renard, G., Rostirolla, D. C., Petersen, G. O., Nunes, J. E., de Souza, A. P., de O Dias, A. C., Chies, J. M., Basso, L. A., Santos, D. S., and Bizarro, C. V. (2014) Production of recombinant human annexin V by fed-batch cultivation. *BMC Biotechnol.* **14,** 33–33 CrossRef Medline
22. Maurer-Fogy, I., Reutelingsperger, C. P., Pieters, J., Bodo, G., Stratowa, C., and Hauptmann, R. (1988) Cloning and expression of cDNA for human vascular anticoagulant, a Ca^{2+}-dependent phospholipid-binding protein. *Eur. J. Biochem.* **174,** 585–592 CrossRef Medline
23. Liang, P., Zhang, X., and Jing, J. (2009) The recombinant expression and properties of human annexin V. *J. Beijing Normal Univ.* (*Natur. Sci.*) **45,** 378–380
24. Flaherty, M. J., West, S., Heimark, R. L., Fujikawa, K., and Tait, J. F. (1990) Placental anticoagulant protein-I: measurement in extracellular fluids and cells of the hemostatic system. *J. Lab. Clin. Med.* **115,** 174–181 Medline
25. Fox, S. C., Sasae, R., Janson, S., May, J. A., and Heptinstall, S. (2004) Quantitation of platelet aggregation and microaggregate formation in whole blood by flow cytometry. *Platelets* **15,** 85–93 CrossRef Medline
26. Chen, Y. C., Cheng, C. H., Shiu, J. H., Chang, Y. T., Chang, Y. S., Huang, C. H., Lee, J. C., and Chuang, W. J. (2012) Expression in *Pichia pastoris* and characterization of echistatin, an RGD-containing short disintegrin. *Toxicon* **60,** 1342–1348 CrossRef Medline
27. Kenis, H., and Reutelingsperger, C. (2009) Targeting phosphatidylserine in anticancer therapy. *Curr. Pharm. Des.* **15,** 2719–2723 CrossRef Medline
28. Tait, J. F., Cerqueira, M. D., Dewhurst, T. A., Fujikawa, K., Ritchie, J. L., and Stratton, J. R. (1994) Evaluation of annexin V as a platelet-directed thrombus targeting agent. *Thromb. Res.* **75,** 491–501 CrossRef Medline
29. Li, C., Huang, J., and Yang, G. (2001) A rabbit femoral artery thrombosis model induced by balloon injury. *J. Nanjing Med. Univ.* **21,** 277–280

30. Reutelingsperger, C. P., Kop, J. M., Hornstra, G., and Hemker, H. C. (1988) Purification and characterization of a novel protein from bovine aorta that inhibits coagulation. Inhibition of the phospholipid-dependent factor-Xa–catalyzed prothrombin activation, through a high-affinity binding of the anticoagulant to the phospholipids. *Eur. J. Biochem.* **173,** 171–178 CrossRef Medline
31. Monroe, D. M., Hoffman, M., and Roberts, H. R. (2002) Platelets and thrombin generation. *Arterioscler. Thromb. Vasc. Biol.* **22,** 1381–1389 CrossRef Medline
32. Lane, D. A., Philippou, H., and Huntington, J. A. (2005) Directing thrombin. *Blood* **106,** 2605–2612 CrossRef Medline
33. Lord, S. T. (2007) Fibrinogen and fibrin: scaffold proteins in hemostasis. *Curr. Opin. Hematol.* **14,** 236–241 CrossRef Medline
34. van Heerde, W. L., Poort, S., van 't Veer, C., Reutelingsperger, C. P., and de Groot, P. G. (1994) Binding of recombinant annexin V to endothelial cells: effect of annexin V binding on endothelial-cell-mediated thrombin formation. *Biochem. J.* **302,** 305–312 CrossRef Medline
35. van Genderen, H. O., Kenis, H., Hofstra, L., Narula, J., and Reutelingsperger, C. P. (2008) Extracellular annexin A5: functions of phosphatidylserine-binding and two-dimensional crystallization. *Biochim. Biophys. Acta* **1783,** 953–963 CrossRef Medline
36. Oling, F., and Bergsma-Schutter, W., and Brisson, A. (2001) Trimers, dimers of trimers, and trimers of trimers are common building blocks of annexin a5 two-dimensional crystals. *J. Struct. Biol.* **133,** 55–63 CrossRef Medline
37. Andree, H. A., Stuart, M. C., Hermens, W. T., Reutelingsperger, C. P., Hemker, H. C., Frederik, P. M, and Willems, G. M. (1992) Clustering of lipid-bound annexin V may explain its anticoagulant effect. *J. Biol. Chem.* **267,** 17907–17912 Medline
38. Tait, J. F., Engelhardt, S., Smith, C., and Fujikawa, K. (1995) Prourokinase-annexin V chimeras. Construction, expression, and characterization of recombinant proteins. *J. Biol. Chem.* **270,** 21594–21599 CrossRef Medline
39. Tanaka, K., Einaga, K., Tsuchiyama, H., Tait, J. F., and Fujikawa, K. (1996) Preparation and characterization of a disulfide-linked bioconjugate of annexin V with the B-chain of urokinase: an improved fibrinolytic agent targeted to phospholipid-containing thrombi. *Biochemistry* **35,** 922–929 CrossRef Medline
40. Yuan, H., Yang, X., and Hua, Z. C. (2004) Optimization of expression of an annexin V-hirudin chimeric protein in *Escherichia coli*. *Microbiol. Res.* **159,** 147–156 CrossRef Medline
41. Chen, H. H., Vicente, C. P., He, L., Tollefsen, D. M., and Wun, T. C. (2005) Fusion proteins comprising annexin V and Kunitz protease inhibitors are highly potent thrombogenic site-directed anticoagulants. *Blood* **105,** 3902–3909 CrossRef Medline
42. Huang, X., Ding, W. Q., Vaught, J. L., Wolf, R. F., Morrissey, J. H., Harrison, R. G., and Lind, S. E. (2006) A soluble tissue factor-annexin V chimeric protein has both procoagulant and anticoagulant properties. *Blood* **107,** 980–986 Medline
43. Kuypers, F. A., Larkin, S. K., Emeis, J. J., and Allison, A. C. (2007) Interaction of an annexin V homodimer (Diannexin) with phosphatidylserine on cell surfaces and consequent antithrombotic activity. *Thromb. Haemost.* **97,** 478–486 CrossRef Medline
44. Gan, Z. R., Gould, R. J., Jacobs, J. W., Friedman, P. A., and Polokoff, M. A. (1988) Echistatin. A potent platelet aggregation inhibitor from the venom of the viper, *Echis carinatus*. *J. Biol. Chem.* **263,** 19827–19832 Medline
45. Tcheng, J. E. (1996) Glycoprotein IIb/IIIa receptor inhibitors: putting the EPIC, IMPACT II, RESTORE, and EPILOG trials into perspective. *Am. J. Cardiol.* **78,** 35–40 Medline
46. Nguyen-Ho, P., and Lakkis, N. M. (2001) Platelet glycoprotein IIb/IIIa receptor antagonists and coronary artery disease. *Curr. Atheroscler. Rep.* **3,** 139–148 CrossRef Medline
47. Xu, Q., Yin, J., and Si, L. (2013) Efficacy and safety of early versus late glycoprotein IIb/IIIa inhibitors for PCI. *Int. J. Cardiol.* **162,** 210–219 CrossRef Medline
48. Scarborough, R. M., Naughton, M. A., Teng, W., Rose, J. W., Phillips, D. R., Nannizzi, L., Arfsten, A., Campbell, A. M., and Charo, I. F. (1993) Design of potent and specific integrin antagonists. Peptide antagonists with high specificity for glycoprotein IIb-IIIa. *J. Biol. Chem.* **268,** 1066–1073 Medline
49. Studier, F. W., and Moffatt, B. A. (1986) Use of bacteriophage T7 RNA polymerase to direct selective high-level expression of cloned genes. *J. Mol. Biol.* **189,** 113–130 CrossRef Medline
50. Smith, D. B., and Johnson, K. S. (1988) Single-step purification of polypeptides expressed in *Escherichia coli* as fusions with glutathione *S*-transferase. *Gene* **67,** 31–40 CrossRef Medline
51. Sambrock, J., and Russel, D. W. (2001) *Molecular Cloning: A Laboratory Manual*, 3rd Ed., Cold Spring Harbor Laboratory Press, Cold Spring Harbor, NY
52. Schägger, H. (2006) Tricine-SDS-PAGE. *Nat. Protoc.* **1,** 16–22 CrossRef Medline
53. Bradford, M. M. (1976) A rapid and sensitive method for the quantitation of microgram quantities of protein utilizing the principle of protein-dye binding. *Anal. Biochem.* **72,** 248–254 CrossRef Medline
54. Yi, X., Hao, Y., Xia, N., Wang, J., Quintero, M., Li, D., and Zhou, F. (2013) Sensitive and continuous screening of inhibitors of β-site amyloid precursor protein cleaving enzyme 1 (BACE1) at single SPR chips. *Anal. Chem.* **85,** 3660–3666 CrossRef Medline
55. Yang, C., Wang, J. X., and Han, Y. (2007) Research advance in platelet function assays. *Zhongguo Shi Yan Xue Ye Xue Za Zhi.* **15,** 1130–1134 Medline
56. Dejana, E., Villa, S., and de Gaetano, G. (1982) Bleeding time in rats: a comparison of different experimental conditions. *Thromb. Haemost.* **48,** 108–111 Medline